European Journal of Heart Failure (2013) **15**, 130–140
doi:10.1093/eurjhf/hfs192

Hyperpolarized ^{13}C magnetic resonance reveals early- and late-onset changes to *in vivo* pyruvate metabolism in the failing heart

Marie A. Schroeder[1,2]*, Angus Z. Lau[1,3], Albert P. Chen[4], Yiping Gu[1], Jeevan Nagendran[5], Jennifer Barry[1], Xudong Hu[6], Jason R.B. Dyck[5], Damian J. Tyler[2], Kieran Clarke[2], Kim A. Connelly[1,6], Graham A. Wright[1,3], and Charles H. Cunningham[1,3]

[1]Sunnybrook Health Sciences Centre, 2075 Bayview Avenue, Room M326A, Toronto, Ontario M4N 3M5, Canada; [2]Department of Physiology, Anatomy & Genetics, University of Oxford, UK; [3]Department of Medical Biophysics, University of Toronto, Canada; [4]GE-Healthcare, Toronto, Canada; [5]Departments of Pediatrics and Pharmacology, University of Alberta, Canada; and [6]Keenan Research Centre in the Li Ka Shing Knowledge Institute, St. Michael's Hospital and University of Toronto, Toronto, Canada

Received 13 August 2012; revised 31 August 2012; accepted 7 September 2012; online publish-ahead-of-print 19 December 2012

See page 123 for the editorial comment on this article (doi:10.1093/eurjhf/hfs211)

Aims Impaired energy metabolism has been implicated in the pathogenesis of heart failure. Hyperpolarized ^{13}C magnetic resonance (MR), in which ^{13}C-labelled metabolites are followed using MR imaging (MRI) or spectroscopy (MRS), has enabled non-invasive assessment of pyruvate metabolism. We investigated the hypothesis that if we serially examined a model of heart failure using non-invasive hyperpolarized [^{13}C]pyruvate with MR, the profile of *in vivo* pyruvate oxidation would change throughout the course of the disease.

Methods and results Dilated cardiomyopathy (DCM) was induced in pigs ($n = 5$) by rapid pacing. Pigs were examined using MR at weekly time points: cine-MRI assessed cardiac structure and function; hyperpolarized [2-^{13}C]pyruvate was administered intravenously, and ^{13}C MRS monitored [^{13}C]glutamate production; ^{31}P MRS assessed cardiac energetics [phosphocreatine (PCr)/ATP]; and hyperpolarized [1-^{13}C]pyruvate was administered for MRI of pyruvate dehydrogenase complex (PDC)-mediated pyruvate oxidation via [^{13}C]bicarbonate production. Early in pacing, the cardiac index decreased by 25%, PCr/ATP decreased by 26%, and [^{13}C]glutamate production decreased by 51%. After clinical features of DCM appeared, end-diastolic volume increased by 40% and [^{13}C]bicarbonate production decreased by 67%. Pyruvate dehydrogenase kinase 4 protein increased by two-fold, and phosphorylated *Akt* decreased by half. Peroxisome proliferator-activated receptor-α and carnitine palmitoyltransferase-1 gene expression decreased by a half and a third, respectively.

Conclusion Despite early changes associated with cardiac energetics and ^{13}C incorporation into the Krebs cycle, pyruvate oxidation was maintained until DCM developed, when the heart's capacity to oxidize both pyruvate and fats was reduced. Hyperpolarized ^{13}C MR may be important to characterize metabolic changes that occur during heart failure progression.

Keywords Magnetic resonance

* Corresponding author. Sunnybrook Health Sciences Centre, 2075 Bayview Avenue, Room M326A, Toronto, Ontario M4N 3M5, Canada. Tel: +416 480 6100, ext. 5790, Fax: +416 480 5021, Email: marie.schroeder@dpag.ox.ac.uk

Introduction

There is increasing evidence that changes in metabolic substrate utilization and depleted myocardial energetic reserve may contribute to LV dysfunction in patients with heart failure.[1,2] Abnormal myocardial energy metabolism has been identified in heart failure patients using ^{31}P magnetic resonance spectroscopy (MRS)[3,4] and positron emission tomography (PET).[5,6] Substrate utilization in the failing heart has been associated with a 'fetal' pattern of metabolic gene expression[7,8] that results in the preferential use of carbohydrates over free fatty acids (FFAs) for ATP production.[9–13] This topic remains controversial, however, as other studies have reported that the failing heart preferentially takes up FFAs[14,15] and that the capacity for carbohydrate uptake and/or oxidation in heart failure is reduced,[9] associated with insulin resistance.[16,17] It has also been shown that the relative utilization of fatty acids and glucose shifts depending on the aetiology and stage of disease.[1,16,18]

The controversy over substrate metabolism in heart failure may originate from the limitations of standard methods for assessing myocardial metabolism. For example, *in vitro* measurements of total protein or mRNA content do not necessarily reflect metabolic activity, and enzyme assays performed in homogenized tissue samples may be misleading owing to the maximal/unphysiological substrate and hormone levels used in the assay, compared with *in vivo*. Radiolabelled tracer imaging techniques, including PET and single photon emission computed tomography (SPECT), cannot distinguish between the injected tracer and its downstream metabolic products and they use ionizing radiation.[19] To understand the timing and consequences of switches in substrate metabolism during heart failure, and potentially to use those switches to diagnose disease severity and optimize treatment, a non-invasive method capable of serially monitoring cardiac metabolism *in vivo* is required.[20]

Magnetic resonance imaging and spectroscopy (MRI and MRS) have long been used to monitor cardiac structure and function non-invasively at repeated times and various stages of disease. The application of MR for metabolic imaging, however, has been limited by intrinsically low sensitivity. Hyperpolarization using the dynamic nuclear polarization (DNP) technique is a process that can yield >10 000-fold signal increases in MR-active nuclei.[21] When used with MRI and MRS, hyperpolarized ^{13}C-labelled tracers allow non-invasive visualization of normal and abnormal metabolism.[22–24]

We hypothesized that, if we serially examined a model of heart failure using non-invasive hyperpolarized [^{13}C]pyruvate with MR, the pattern of pyruvate oxidation by the enzyme complex pyruvate dehydrogenase (PDC) and the Krebs cycle would change throughout the course of the disease. Furthermore, by using hyperpolarized ^{13}C MR alongside MR-based measurements of cardiac energetics, structure, and contractile function, and *in vitro* measurements of ATP content and gene/protein expression, we aimed to enhance our understanding of how altered metabolic fluxes contribute to heart failure pathogenesis.

To test our hypothesis, we examined a porcine pacing model of dilated cardiomyopathy (DCM) using clinically applicable hyperpolarized ^{13}C MRS and MRI methods, with the tracers [1-^{13}C]pyruvate and [2-^{13}C]pyruvate. Serial MR was applied for non-invasive assessment of cardiac structure, function, energetics, and pyruvate metabolism, in normal hearts and throughout the development of heart failure (*Figure 1*). Hyperpolarized ^{13}C MRS identified an early-onset change to Krebs cycle-mediated ^{13}C accumulation in the glutamate pool, and a late-onset reduction in hyperpolarized [1-^{13}C]pyruvate oxidation via PDC. This work has provided the first evidence that metabolic imaging using hyperpolarized ^{13}C MR may be a useful tool to diagnose disease severity and optimize treatment for heart failure patients, an important result as clinical application of hyperpolarized ^{13}C MR in cardiovascular patients is positioned to occur in the near future.[25]

Methods

Study overview

Dilated cardiomyopathy was induced in female Yorkshire pigs ($n = 5$, 20 kg at baseline, 1 month old) by chronic rapid right ventricular (RV) pacing. After allowing pigs to recover from pacemaker implantation for >1 week, pacemakers were set to beat at 188 b.p.m. until pigs developed heart failure. At baseline and at weekly intervals throughout the duration of the pacing protocol, MR was used to examine *in vivo* cardiac physiology in each pig (details below). Pigs were sacrificed at the first MR examination point at which they already displayed clinical signs of heart failure, including discoloured skin and mucosal membranes, dyspnoea, pulmonary oedema, myocardial dilatation, ascites, and peripheral oedema.

All MR experiments were performed on a GE MR750 3T MR scanner. After each pig was positioned in the magnet, proton cine-MR images were acquired. During cine-MRI, the [2-^{13}C]pyruvate was hyperpolarized,[26] and venous blood from the pig was taken for biochemical analyses. Once cine images were acquired, a dose of hyperpolarized [2-^{13}C]pyruvate was dissolved and infused into the pig ear vein while ^{13}C MR spectra were acquired. Next, in the interval during which [1-^{13}C]pyruvate was hyperpolarized, ^{31}P spectra were acquired. Finally, hyperpolarized [1-^{13}C]pyruvate was infused while ^{13}C metabolic images were acquired.[27]

Dynamic nuclear polarization with dissolution[21,27,28] was used to generate both aqueous hyperpolarized [2-^{13}C]pyruvate (for MRS experiments) and [1-^{13}C]pyruvate (for MRI experiments). For both sets of experiments, 0.05 mmol/kg of hyperpolarized [^{13}C]pyruvate was injected over 15 s into the right ear vein, and scanning was initiated at the beginning of the infusion.

An overview of the experimental protocol is presented in *Figure 1*. A description of each MR acquisition is detailed below, and the procedures used for [^{13}C]pyruvate polarization and dissolution, MR data analysis, and for biopsy and heart tissue analyses are described further in the Supplementary material. Primer sequences designed in-house and used for real-time quantitative PCR (qRT-PCR) are given in Supplementary material, *Table S2*. All animal experiments were performed between 13:00 and 17:00 h and were carried out under a protocol approved by the institutional animal care and use committee.

Magnetic resonance imaging and spectroscopy

Proton cine-magnetic resonance imaging

To assess cardiac structure and function, cardiac-gated breath-held steady-state free precession (SSFP) cine images were acquired in the

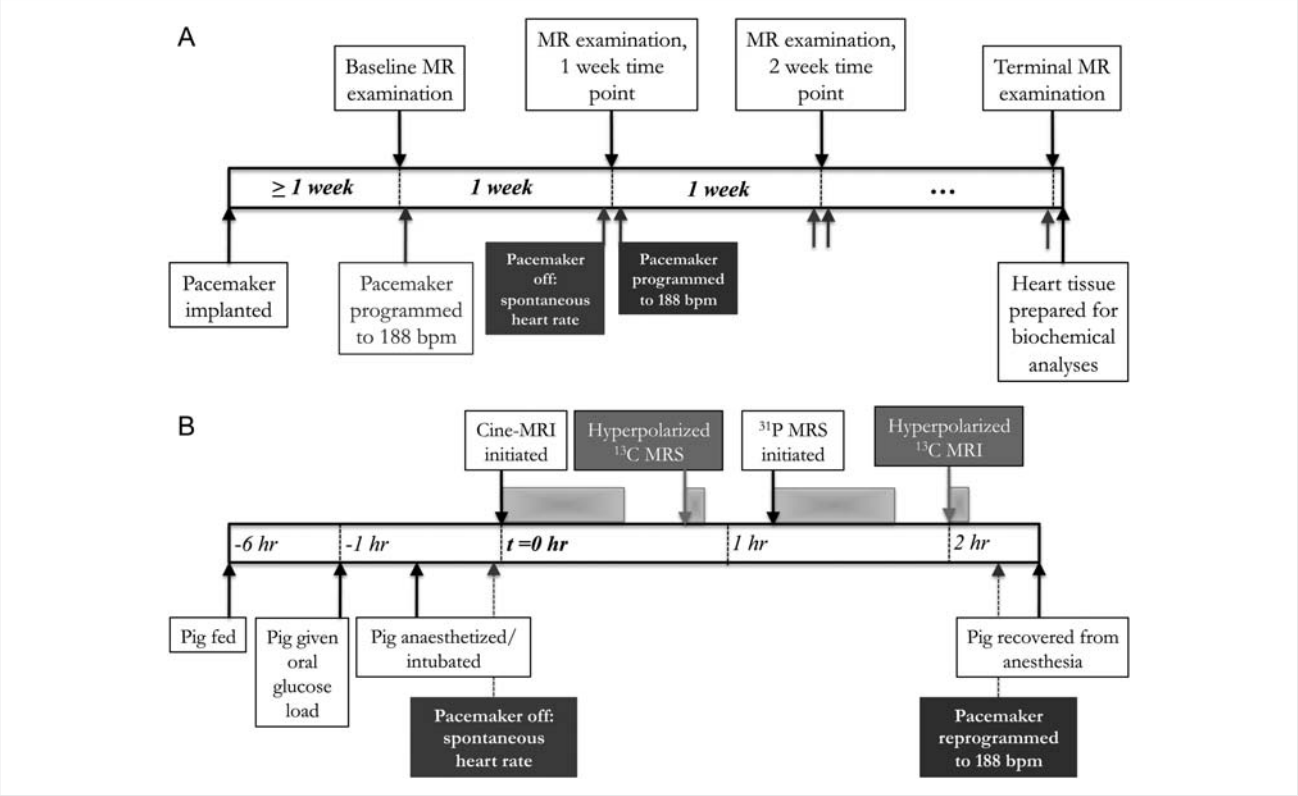

Figure 1 An overview of the experimental protocol, applied to each of the pigs ($n = 5$). The top time line (*A*) shows that each pig was examined at weekly intervals, whereas the bottom time line (*B*) shows the magnetic resonance (MR) scans performed at each examination point. (*A*) After pacemaker implantation, the pig was examined at baseline, before the pacemaker was programmed to 188 b.p.m. Pigs were examined using MR imaging (MRI) and MR spectroscopy (MRS) at weekly intervals, until heart failure developed (~5 weeks of pacing). After the pig began to display clinical signs of heart failure, a terminal examination was performed, the pig was sacrificed, and myocardial tissue was harvested. (*B*) Each MR examination consisted of: (i) metabolic preparation, which consisted of a 5 h fast and an oral glucose load given 1 h prior to MR examination; (ii) anaesthesia, cessation of pacing, and positioning in the MR scanner; (iii) Cine-MRI; (iv) infusion of hyperpolarized [2-^{13}C]pyruvate and MRS; (v) ^{31}P MRS; and (vi) infusion of hyperpolarized [1-^{13}C]pyruvate and ^{13}C MRI.

short-axis view [repetition time (TR) = 4.2 ms, echo time (TE) = 1.8 ms, field of view (FOV) 24 cm, slice thickness 5 mm, spacing 5 mm, matrix size 224 × 224] using a ^{1}H surface coil.

Carbon-13 magnetic resonance spectroscopy

Upon infusion of [2-^{13}C]pyruvate,[26] MR spectra were acquired to follow Krebs cycle-mediated conversion into [5-^{13}C]glutamate. A slice-selective, cardiac-gated pulse-and-acquire sequence [slice thickness 10 cm, nominal fractional anisotropy (FA) = 10°] was used to acquire data, using a custom-built transmit/receive 13 cm ^{13}C surface coil. Spatial localization was provided by a combination of the small tip-angle slice-selective sinc excitation pulse and the placement of the ^{13}C surface coil on the chest, over the region where the heart was located. One spectrum (2048 spectral points, 5 kHz bandwidth) was acquired cardiac gated to every three R–R intervals to acquire one time point approximately every 2 s.

Phosphorus-31 magnetic resonance spectroscopy

^{31}P two-dimensional chemical shift imaging (2D-CSI) data were acquired from a 3 cm slice in short-axis view using a cardiac-gated pulse-acquire pulse sequence (16 × 16 matrix, 3 cm in-plane resolution, 45° tip angle, TR = 2R/R, ~1.5 s, four averages), and a 13 cm ^{31}P transmit/receive surface coil.

Carbon-13 magnetic resonance imaging

A chemical shift-specific, cardiac and respiratory-gated ^{13}C MRI sequence was used to image [1-^{13}C]pyruvate, [^{13}C]bicarbonate, and [1-^{13}C]lactate with 9 mm in-plane spatial resolution in two 1 cm slices. Metabolite images were acquired with 2.5 s temporal resolution per set of slices to capture both the time course of the [1-^{13}C]pyruvate bolus and its subsequent metabolism.[27,29] A spectral–spatial pulse was used to select the appropriate resonance for imaging in each frame. Two short-axis images at mid-chamber and apical positions were acquired at end-expiration in diastole. A total of 35 imaging frames were acquired over a total scan time of 1.5 min, as follows: 10 frames (7.5° tip angle) to capture the first pass of the [1-^{13}C] pyruvate bolus were acquired, followed by an interleaved set of 25 frames corresponding to bicarbonate (90° tip angle), lactate (90°), and pyruvate (45°).

Data analysis

Pigs took between 4 and 6 weeks of pacing to develop clinical signs of DCM. To allow comparison of all parameters measured for each pig, data were grouped into three time periods. Grouping depended solely on the pacing duration and was performed blinded to data analysis. The first period (early) reflected the physiological changes due to early pacing, and reported an average of data acquired after 1–2 weeks

of pacing. The second period (moderate) reflected a stage of subclinical cardiac dysfunction, and reported an average of data acquired after 2–5 weeks of pacing. The third period (DCM) reflected overt heart failure. Only data taken from the terminal examination point, after our endpoint had been reached, were included in this group (4–6 weeks of pacing).

Proton cine-magnetic resonance imaging

The LV epicardial borders, and the LV and RV endocardial borders were manually outlined in end-diastolic and end-systolic frames. Global end-diastolic volume (EDV), end-systolic volume (ESV), wall thickness, EF, and cardiac output (CO) were calculated. All parameters were indexed to pig body surface area.

Carbon-13 magnetic resonance spectroscopy

For each dynamic series of MR spectra, relative [5-^{13}C]glutamate production was measured by calculating the ratio of the maximum metabolite peak area to the maximum [2-^{13}C]pyruvate peak area, and expressed as a percentage.

Phosphorus-31 magnetic resonance spectroscopy

Spectra were processed to fit for phosphocreatine (PCr), 2,3-diphosphoglycerate, and γ-ATP. Resonance areas were corrected for the effects of saturation and blood contamination to calculate PCr/ATP.[3]

Carbon-13 magnetic resonance imnaging

[1-^{13}C]Pyruvate, ^{13}C-bicarbonate, and [1-^{13}C]lactate images were reconstructed using an automatic off-resonance correction algorithm as described previously.[27] For each set of [^{13}C]bicarbonate and [1-^{13}C]lactate images, the mean metabolite signal per unit volume was computed in the anterior half of the ventricular wall of each pig heart. For each measurement, the signal from the anterior myocardium (as chosen from the anatomical images) was summed, and this number was divided by the area of the region multiplied by the slice thickness. This was measured in the image with maximal [^{13}C]metabolite signal. The resulting [^{13}C]bicarbonate and [1-^{13}C]lactate signals were each normalized to the mean [1-^{13}C]pyruvate signal per unit volume within the LV chamber, also measured from the image with maximal [^{13}C]metabolite signal (i.e. the peak of the bolus[29]). This gave ratio indices of PDC-mediated pyruvate oxidation and lactate production via lactate dehydrogenase (LDH).[25,30]

Statistical analysis

Data are expressed as the mean $\pm$ SEM. A normal distribution was confirmed using a Kolmogorov–Smirnov test. For the longitudinal changes in physiological data and all data resulting from non-invasive MR experiments, repeated measures one-way analysis of variance (ANOVA), followed by a post-hoc paired, two-sided Student's *t*-test with Bonferroni correction for multiple comparisons, was used. An unpaired, two-sided Student's *t*-test was used for comparisons between DCM and control biochemistry data ($n = 5$ in each group). All statistical analyses used GraphPad Prism (GraphPad, La Jolla, CA, USA). Significant changes were considered for $P < 0.05$.

Results

Pacing-induced dilated cardiomyopathy

Pigs developed heart failure after 4.6 $\pm$ 0.5 weeks of RV pacing. Physiological parameters at baseline, and as pigs developed DCM, are shown in *Table 1*.

Cine-magnetic resonance imaging

Cine-MRI revealed substantial changes to LV and RV structure and function with the development of heart failure, as described in *Figure 2* and in the Supplementary material, *Table S1*.

Phosphorus-31 magnetic resonance spectroscopy

A representative ^{31}P spectrum, taken from a voxel placed in the *in vivo* pig heart 2 weeks after pacing, is shown in the Supplementary material, *Figure S1*. ^{31}P MRS revealed that myocardial PCr/ATP was progressively depleted throughout the pacing protocol, from 2.3 $\pm$ 0.2 at baseline to 1.7 $\pm$ 0.1 at early pacing, and further to 1.3 $\pm$ 0.2 with moderate subclinical dysfunction (Supplementary material, *Figure S1*). In DCM, ^{31}P MR spectra had a low signal-to-noise ratio to the extent that they were not reproducibly quantifiable, presumably due to the depletion of ATP in

Table 1 Physiological parameters with the development of heart failure

	Baseline	Early	Moderate	DCM
Heart rate, b.p.m.	118 $\pm$ 9	89 $\pm$ 7*	85 $\pm$ 5*	86 $\pm$ 5*
Body weight, kg	25 $\pm$ 2	30 $\pm$ 2	34 $\pm$ 2*	35 $\pm$ 3*
Body surface area, m^2	0.60 $\pm$ 0.03	0.68 $\pm$ 0.02	0.74 $\pm$ 0.02*	0.76 $\pm$ 0.04*
Creatinine, μmol/L	106 $\pm$ 9	126 $\pm$ 17	160 $\pm$ 17	178 $\pm$ 23*
Urea, mmol/L	4.6 $\pm$ 0.6	5.0 $\pm$ 0.4	5.5 $\pm$ 0.5	5.9 $\pm$ 0.3*
Cholesterol, mmol/L	2.3 $\pm$ 0.2	1.9 $\pm$ 0.2	1.9 $\pm$ 0.1	1.4 $\pm$ 0.3*
Glucose, mmol/L	5.3 $\pm$ 0.9	4.6 $\pm$ 0.5	4.8 $\pm$ 0.5	5.3 $\pm$ 0.8
Insulin, pmol/L	57 $\pm$ 13	53 $\pm$ 8	47 $\pm$ 8	59 $\pm$ 9
FFAs, mmol/L	0.11 $\pm$ 0.03	0.16 $\pm$ 0.04	0.07 $\pm$ 0.03	0.07 $\pm$ 0.04
Triglycerides, mmol/L	0.30 $\pm$ 0.10	0.28 $\pm$ 0.06	0.30 $\pm$ 0.07	0.13 $\pm$ 0.06*

DCM, dilated cardiomyopathy; FFAs, free fatty acids.
*$P < 0.05$ compared with baseline.

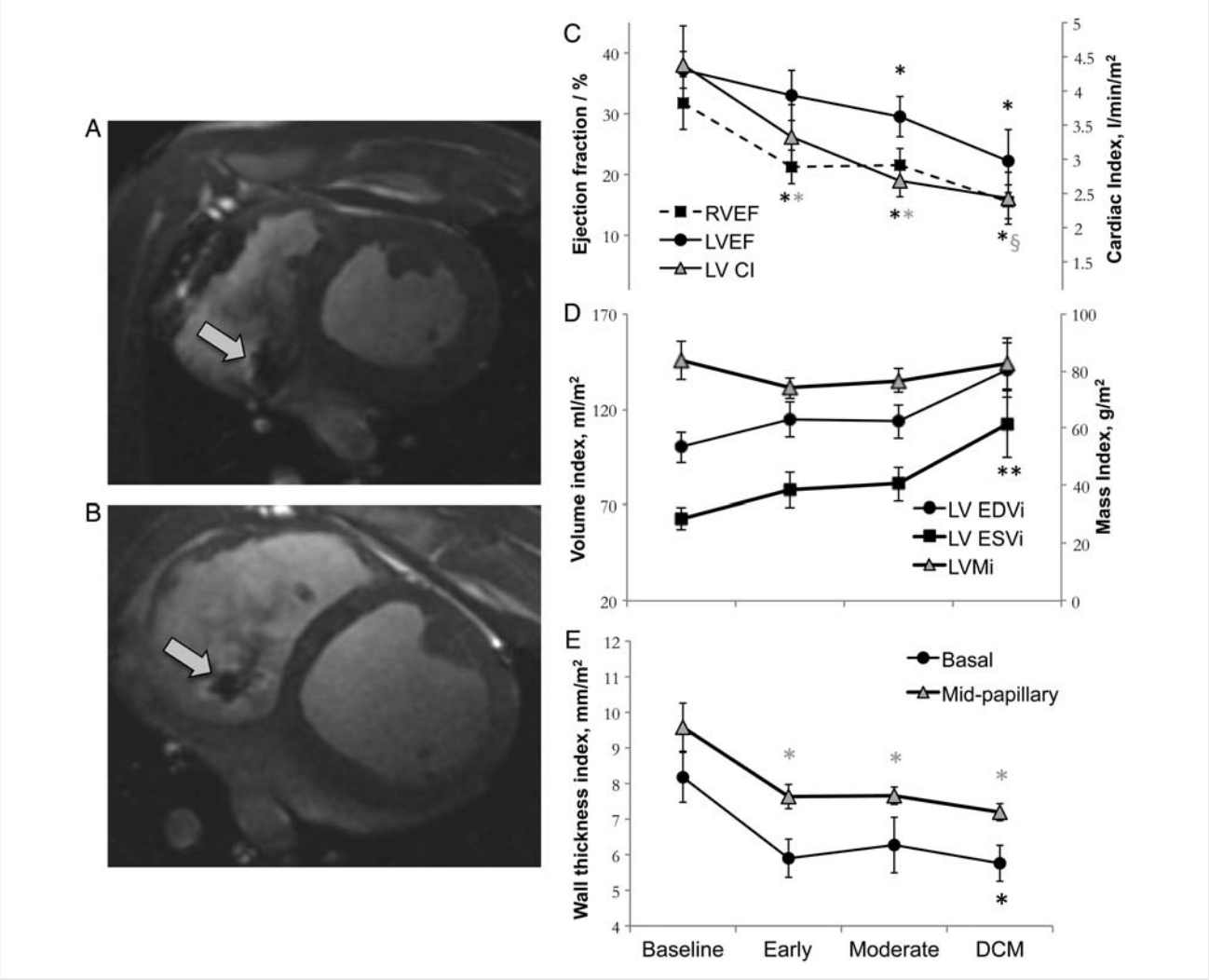

Figure 2 Changes in cardiac structure and function during the development of dilated cardiomyopathy (DCM), measured using cine-magnetic resonance imaging (MRI). Representative images of a mid-papillary slice in diastole from the same pig, acquired at baseline (*A*), and in overt DCM (*B*). An artefact from the right ventricular (RV) pacing lead is visible in both images as indicated by the arrows. Changes in cardiac EF and cardiac index (CI) (*C*), volumes (*D*), and diastolic wall thickness (*E*), in all five pigs. *$P < 0.05$ compared with baseline; §$P < 0.05$ compared with the early time point. EDVi, end-diastolic volume index; EDSi, end-systolic volume index; LVMi, LV mass index.

pacing-induced DCM, measured here (see below) and previously,[4] to decrease its MR signal.

Hyperpolarized ^{13}C magnetic resonance imaging and magnetic resonance spectroscopy

Hyperpolarized ^{13}C magnetic resonance spectroscopy

A representative MR spectrum is shown in *Figure 3A*, with peaks from the infused [2-^{13}C]pyruvate, as well as the metabolic products [5-^{13}C]glutamate (183 p.p.m.) and [1-^{13}C]acetylcarnitine (175 p.p.m., not quantifiable with moderate cardiac dysfunction and DCM). Peak assignments were made by comparison with previous [2-^{13}C]pyruvate studies performed *ex vivo* and *in vivo* in rats.[26,31]

The effects of early pacing, moderate dysfunction, and DCM on cardiac [5-^{13}C]glutamate production are shown in *Figure 3*. At the baseline time point, the maximum [5-^{13}C]glutamate/[2-^{13}C]pyruvate ratio was 4.3 $\pm$ 0.9%. Early after the onset of pacing, the [5-^{13}C]glutamate/[2-^{13}C]pyruvate ratio was reduced by 51%, to 2.1 $\pm$ 0.6%, and stayed at this level throughout disease progression ($P < 0.05$).

As described previously[26,31] and in *Figure 3*, the production of [5-^{13}C]glutamate from [2-^{13}C]pyruvate resulted from (i) PDC-mediated formation of [1-^{13}C]acetyl-CoA; (ii) ^{13}C flux through the first span of the Krebs cycle, into mitochondrial α-ketoglutarate; (iii) ^{13}C flux through the oxoglutarate−malate carrier (OMC), instead of via the Krebs cycle enzyme α-ketoglutarate dehydrogenase (αKGDH); and finally (iv) conversion of [^{13}C] α-ketoglutarate into [5-^{13}C]glutamate. The change to [5-^{13}C] glutamate production in the absence of altered PDC-mediated pyruvate oxidation (see below) indicated either that the relationship between Krebs cycle and OMC fluxes

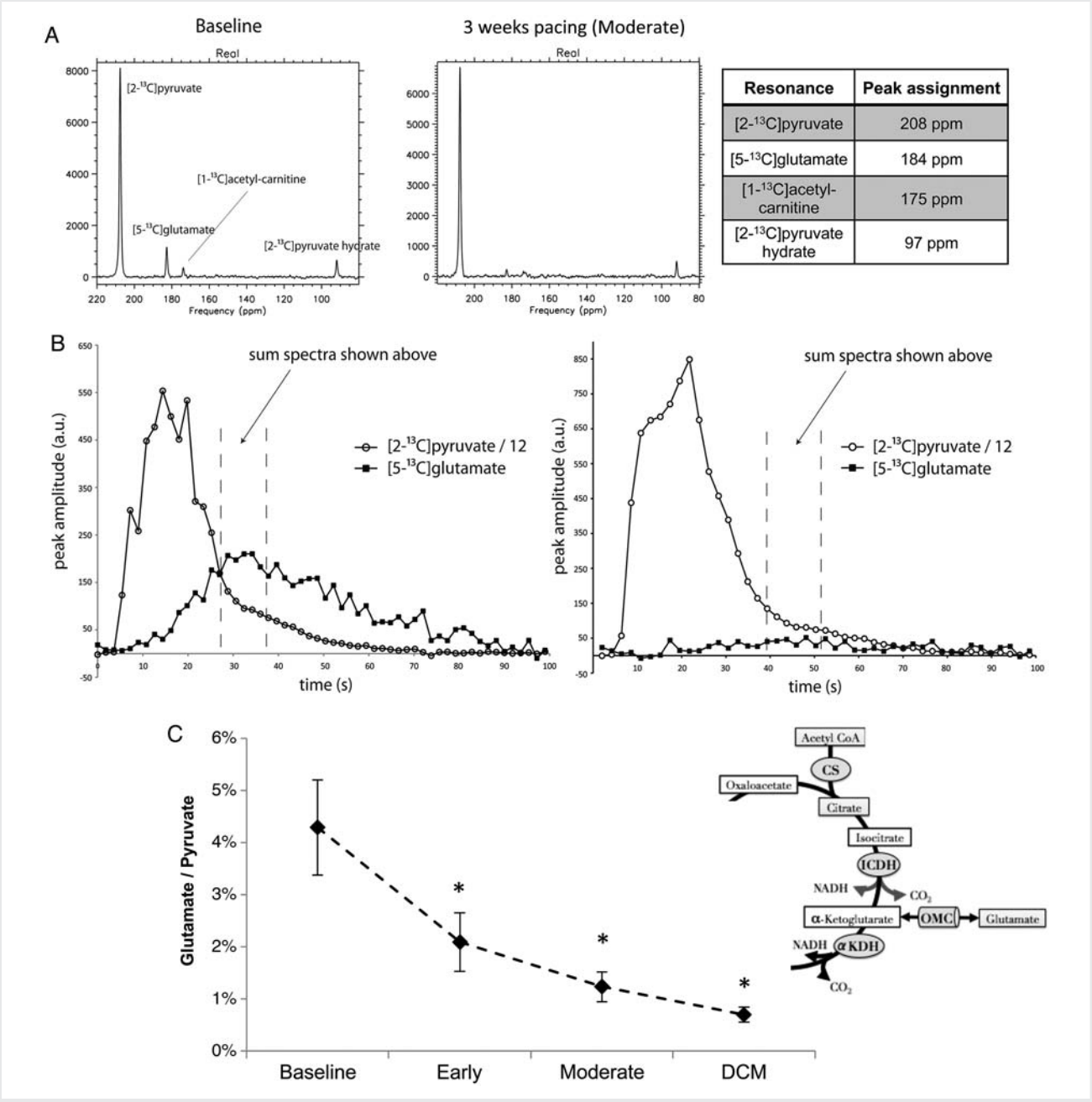

Figure 3 Hyperpolarized ^{13}C magnetic resonance spectroscopy (MRS) showing altered [5-^{13}C]glutamate production during development of dilated cardiomyopathy (DCM), following infusion of hyperpolarized [2-^{13}C]pyruvate. (*A*) Representative spectra taken from a healthy pig (left), and from the same pig after 3 weeks of pacing, when it had moderate cardiac dysfunction. (*B*) Representative time courses of the infused [2-^{13}C]pyruvate and its conversion into [5-^{13}C]glutamate, following quantification of the spectra shown in A. (*C*) The [5-^{13}C]glutamate/[2-^{13}C]pyruvate ratio, measured for all pigs during development of DCM.

changed early after the onset of pacing, or that the glutamate pool size was depleted.

Hyperpolarized ^{13}C magnetic resonance imaging

Figure 4A shows representative *in vivo* images of infused [1-^{13}C]pyruvate and its metabolism into [^{13}C]bicarbonate and [1-^{13}C]lactate. Visual inspection of images (shown in *Figure 4A*) indicated that less of the infused bolus of hyperpolarized [1-^{13}C]pyruvate reached the left ventricle in hearts with DCM. Maximum [^{13}C]bicarbonate signal production across the anterior wall of the myocardium was normalized to LV [1-^{13}C]pyruvate to give a qualitative index of pyruvate oxidation by the PDC.[32] At baseline, [^{13}C]bicarbonate/[1-^{13}C]pyruvate yielded a value of 0.016 $\pm$ 0.002, which remained constant through early pacing and with

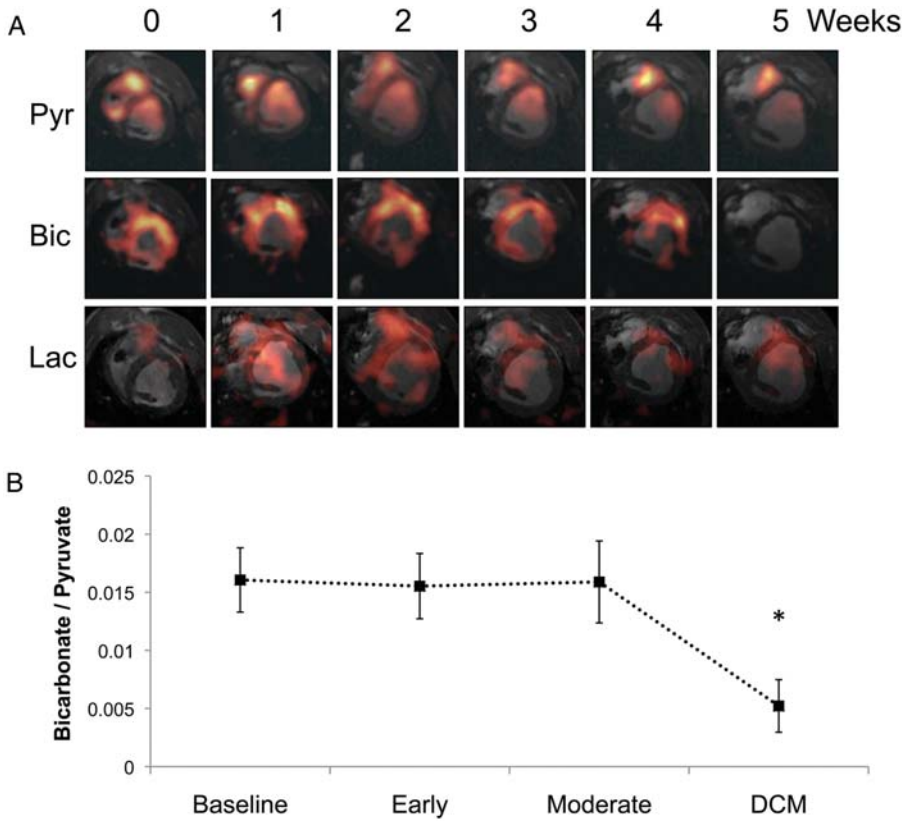

Figure 4 Hyperpolarized ^{13}C magnetic resonance imaging (MRI) results describing alterations to pyruvate dehydrogenase complex (PDC) flux and [^{13}C]lactate production with the pathogenesis of dilated cardiomyopathy (DCM), following infusion of hyperpolarized [1-^{13}C]pyruvate. (*A*) Representative pyruvate (Pyr, top), bicarbonate (Bic, middle), and lactate (Lac, bottom) ^{13}C MR images taken from the same pig and at weekly intervals during the pacing protocol, until DCM developed. The images displayed for each metabolite were selected from the same, mid-papillary slice and in the same respiratory cycle. Signal intensity in the pyruvate image was scaled based on 15–100% of the maximum pyruvate signal at week 0, whereas the bicarbonate and lactate signal intensities were scaled based on 15–100% of the maximum bicarbonate signal intensity at week 0. (*B*) Relative changes to PDC flux with DCM in five pigs.

the development of moderate dysfunction. However, with the development of DCM, the [^{13}C]bicarbonate/[1-^{13}C]pyruvate ratio was reduced by 67% to 0.005 $\pm$ 0.002, suggesting that PDC flux was also reduced (*Figure 4B*). The myocardial [1-^{13}C]lactate/[1-^{13}C]pyruvate level remained constant throughout the duration of the pacing protocol, suggesting no change to LDH flux.

The metabolite signal shown in *Figure 4A* was observed to vary with distance from the chest wall in the manner expected when using a surface coil for both radiofrequency excitation and signal reception, as was done in these experiments. This variation in signal was consistent with the measured spatial profile of this RF coil, as measured in Lau *et al.*[33]. There is also a patchy appearance to the [^{13}C]bicarbonate signal, consistent with the relatively low signal-to-noise ratio in these images. The analysis method used to derive the [^{13}C]bicarbonate/[1-^{13}C]pyruvate ratio, as detailed in 'Data analysis', was insensitive to these spatial variations because the mean signal over a large region of the heart was used, and the coil positioning relative to the heart was similar across the different animals and examination points.

In vitro heart tissue analysis

After the development of DCM, myocardial ATP levels as assessed by a luciferase assay decreased by 41%, from 34.2 $\pm$ 4.0 to 20.2 $\pm$ 2.2 pmol/μg protein. Protein content of phosphorylated *Akt* decreased by half. Pyruvate dehydrogenase kinase 4 (PDK4), normalized to glyceraldehyde 3-phosphate dehydrogenase (GAPDH) protein content, was increased by nearly two-fold (*Figure 5*). Additionally, expression of the genes encoding peroxisome proliferator-activated receptor-α (PPARα) and its downstream target carnitine palmitoyltransferase-1 (CPT1; normalized to GAPDH) was significantly lower in DCM by 50% and 32%, respectively.

Importantly, expression of the gene encoding sarcolemmal pyruvate transporter MCT1 was unchanged with DCM development. Total protein contents of the $E_1\alpha$ subunit of the PDC, LDH B, and glucose transporters 1 and 4 (GLUT1 and GLUT4) were also unchanged between healthy and failing hearts. Phosphorylation of both AS160 (*Akt* substrate of 160 kDa), and 5' AMP-activated protein kinase (AMPK) was unchanged in DCM, with the latter observation further evidenced by the lack of

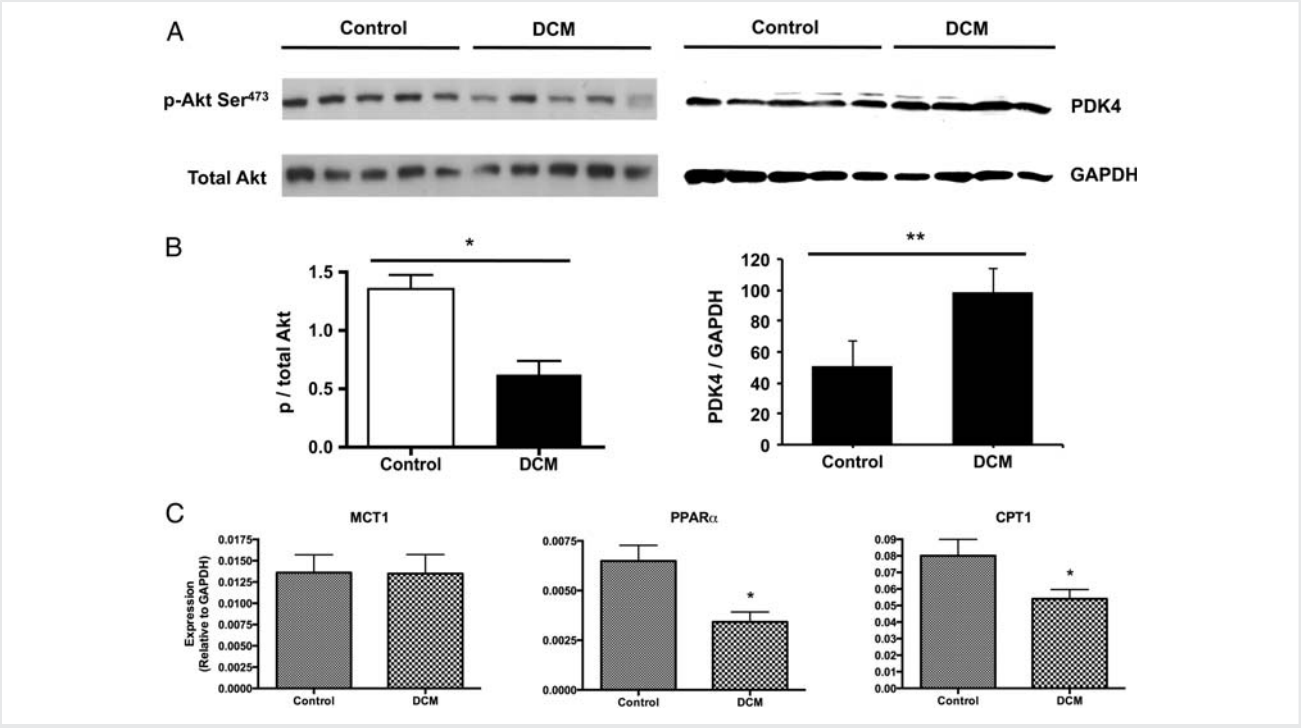

Figure 5 (*A* and *B*) Alterations to myocardial proteins involved in carbohydrate metabolism, in control pigs and in pigs with dilated cardiomyopathy (DCM). The blot for p-*Akt* was normalized to the total *Akt-1* protein content. The blot for pyruvate dehydrogenase kinase 4 (PDK4) was normalized to glyceraldehyde 3-phosphate dehydrogenase (GAPDH) protein, run on the same membrane. (*C*) Alterations to myocardial genes involved in fatty acid oxidation, normalized to GAPDH mRNA, in pigs with DCM. MCT1, monocarboxylate transporter 1; PPARα, peroxisome proliferator-activated receptor-α; CPT1, carnitine palmitoyltransferase-1. *$P < 0.05$; **$P < 0.005$.

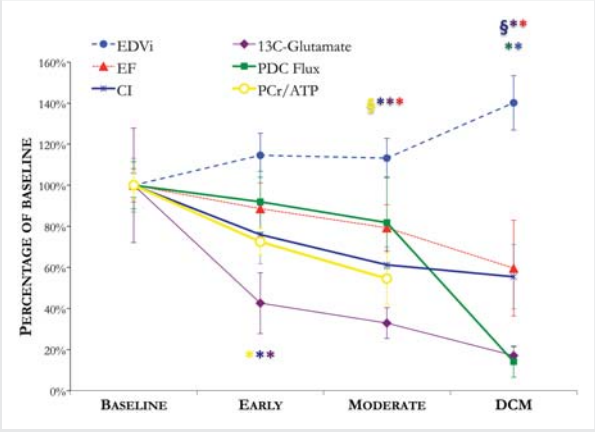

Figure 6 An overview of LV metabolic, energetic, structural, and functional remodelling, measured non-invasively using magnetic resonance imaging (MRI) and magnetic resonance spectroscopy (MRS), throughout the development of tachycardia-induced dilated cardiomyopathy (DCM). *$P < 0.05$ compared with baseline; §$P < 0.05$ compared with the early time point. CI, cardiac index; EDVi, end-diastolic volume index; PCr, phosphocreatine; PDC, pyruvate dehydrogenase complex.

change in genes encoding the AMPK downstream target acetyl-CoA carboxylase (ACC). Finally, gene expression of PGC1-α and PGC1-β was also unchanged in failing hearts.

Discussion

Here, we proved our initial hypothesis to be true: *in vivo*, in a clinically relevant large animal model, hyperpolarized ^{13}C MR uncovered that the profile of pyruvate metabolism varied with the development of heart failure. Specifically, flux of pyruvate through the first span of the Krebs cycle and the OMC changed from baseline to the earliest stage of cardiomyopathy, and pyruvate oxidation by the PDC changed between moderate cardiomyopathy and the onset of DCM. After 1–2 weeks of rapid pacing, we observed reduced [^{13}C]glutamate production from hyperpolarized [2-^{13}C]pyruvate; the physiological significance of this change was indicated by concomitant decreases in both cardiac index (CI) and energy reserve (PCr/ATP). Continued pacing into moderate dysfunction (2–5 weeks) did not alter pyruvate metabolism further, but decreased PCr/ATP and EF significantly. After the onset of heart failure (4–6 weeks), when clinical features of the disease were observed alongside LV wall thinning, dilatation, and further functional impairment, the *in vivo* bicarbonate/

[1-^{13}C]pyruvate ratio decreased dramatically, suggesting reduced capacity for pyruvate oxidation by the PDC.[23,32] PDK4 protein levels were increased, ATP levels were reduced, and activation of both *Akt* and PPARα was reduced. An overview of LV remodelling in DCM is shown in *Figure 6*.

Early-onset metabolic perturbations

At an early stage of cardiomyopathy, ^{13}C incorporation into the glutamate pool was reduced by 51%, the PCr/ATP ratio was reduced by 26%, and while CI was reduced by 25%, neither EF nor cardiac structure yet showed any change. The non-invasive nature of our study precluded collection of myocardial biopsies during DCM development, so validating the physiological mechanism altering [^{13}C]glutamate production was outside the scope of this study. With further validation in future, however, these results could have two potential clinical applications: first, [^{13}C]glutamate production could be an early diagnostic biomarker for aetiologies of heart failure characterized by energetic depletion. Secondly, altered mitochondrial energy metabolism may have had a causal role in heart failure pathogenesis.

Altered metabolism in dilated cardiomyopathy

Our results showed that *in vivo*, oxidation of [1-^{13}C]pyruvate by the PDC was maintained throughout early and moderate cardiomyopathy. Additionally, in DCM, we measured reduced ATP content, and reduced expression of the genes encoding the regulator of fatty acid oxidation, PPARα, and its downstream target CPT1. These observations were consistent with many studies performed in patients and in experimental models, which have suggested that the failing heart is reliant on glucose metabolism due to decreased capacity for ATP generation via fatty acid oxidation.[1,2,7,9–13]

In DCM, however, hyperpolarized ^{13}C MRI revealed a 67% reduction to *in vivo* oxidation of [1-^{13}C]pyruvate by the PDC. This agrees with a study performed in cardiomyopathic hamsters showing reduced PDC activity.[34] Furthermore, because hyperpolarized ^{13}C MRI enabled serial measurements throughout disease pathogenesis, this is the first study to identify a temporal association between altered cardiac PDC flux and the transition to decompensated heart failure.[2] Our data suggest that failing hearts compensated throughout early and moderate pacing via an increased reliance on carbohydrate oxidation via the PDC to produce ATP, depleting the energetic reserve (PCr/ATP) without major detriment to contractility or geometry (*Figure 6*). Ultimately, hearts may have failed when they lost the ability to use pyruvate as fuel to generate ATP in the context of already reduced fatty acid oxidation capacity.

Biochemical analyses helped to clarify the mechanisms contributing to decreased *in vivo* cardiac PDC flux. Though total expression of the $E_1\alpha$ subunit of the PDC was unchanged in DCM, protein expression of PDK4, which phosphorylates and inhibits PDC, was elevated by 94%. Therefore, we expect that PDK4-mediated inhibition contributed to the reduced *in vivo* [^{13}C]bicarbonate production from PDC.

Dilated cardiomyopathy decreased *Akt* phosphorylation by 54%. This finding agreed with a study by Nikolaidis *et al.*, which confirmed that *Akt* phosphorylation was reduced due to increased phosphatase and tensin homologue (PTEN) phosphatase expression in tachycardia-induced DCM, resulting in impaired GLUT4 translocation to the sarcolemma, defective myocardial insulin signalling, and whole-body insulin resistance.[16] As insulin directly activates PDC via protein kinase C-δ and pyruvate dehydrogenase phosphatase (PDP),[38] defective myocardial insulin signalling may have also contributed to the reduction in PDC-mediated [1-^{13}C]pyruvate oxidation that we observed.

This study has revealed the importance of serially assessing pyruvate metabolism under *in vivo* conditions, at frequent time points as heart failure progresses. We saw that the capacity for PDC to oxidize pyruvate changed dramatically over just 1 week, with no contribution from anaplerosis, as the heart transitioned from compensated cardiomyopathy to decompensated DCM. Studies not performed serially throughout DCM development, that simply compared metabolism in healthy subjects and subjects with severe heart failure, may have missed the onset of this change and thus the association between PDC capacity and DCM. Furthermore, studies reporting increased glucose uptake in DCM do not necessarily imply increased glucose oxidation, as PDC activity must also be high for efficient use of glucose as energetic fuel. Our *in vivo* hyperpolarized [1-^{13}C]pyruvate oxidation measurements suggest that treatments that ameliorate insulin resistance (glucagon-like peptide-1 agonists[10]) or block FFA uptake (carnitine palmitoyltransferase-I inhibitors[39]) improve myocardial energetics because they also enhance flux through PDC.

Study limitations

One limitation of this study was that we did not take myocardial tissue samples at each experimental time point. Future biochemical investigation of metabolic alterations occurring after 1–2 weeks of pacing is warranted to determine the mechanism driving reduced [^{13}C]glutamate production. If we can validate this mechanism, in future it may be possible to use [^{13}C]glutamate production as a biomarker to diagnose cardiomyopathy and to optimize its treatment in the clinic.

A second limitation was that the delivery of hyperpolarized [^{13}C]pyruvate to the myocardium and its uptake into cardiomyocytes could have influenced our measurements. Accordingly, we accounted for changes to myocardial blood flow throughout DCM development by dynamically imaging the infused hyperpolarized [^{13}C]pyruvate bolus, and normalizing metabolite signals to the LV signal from infused [^{13}C]pyruvate. To our knowledge, no changes to basal myocardial perfusion have been reported in tachycardia-induced DCM. Further, mRNA encoding the monocarboxylate transporter (MCT,[40] which enables pyruvate uptake into cardiomyocytes) did not change in DCM, suggesting that [^{13}C]pyruvate uptake also remained constant. However, MCT expression increased in heart failure following myocardial infarction,[41] indicating that in other disease aetiologies hyperpolarized ^{13}C MR may overestimate carbohydrate oxidation. In future, this issue can be avoided by using dual-labelled [1, 2-$^{13}C_2$]pyruvate to monitor [^{13}C]glutamate and [^{13}C]bicarbonate production simultaneously.[42] This approach would enable measurement of a [^{13}C]glutamate/[^{13}C]bicarbonate ratio that only considers ^{13}C labels reaching the cardiac mitochondria (illustrated in Supplementary material, *Figure S2*), and would be insensitive to factors such as

[^{13}C]pyruvate delivery, uptake, and blood pool size due to ventricular dilatation.

Significance of this work

Hyperpolarized [1-^{13}C]pyruvate was administered to patients for the first time in 2010, with a view towards using metabolic MRI to characterize prostate cancer. The study presented here offers the first evidence that using hyperpolarized ^{13}C MR to follow cardiovascular disease progression in patients is also feasible. We applied novel hyperpolarized ^{13}C MRI and MRS data acquisition and analysis methods that are promising for direct translation into humans for the following reasons: (i) the dose of [^{13}C]pyruvate tracer was half of the dose that has been used in the first patient study; (ii) we acquired cardiac-gated ^{13}C MRI and MRS data from free-breathing pigs on a standard whole-body MR scanner, using a sequence that could easily be implemented in free-breathing patients;[29] (iii) dynamic imaging of the [1-^{13}C]pyruvate input bolus[29] enabled ratiometric data analysis, which accounted for the altered tracer pharmacokinetics that occur with disease; and (iv) each ^{13}C scan was completed within ~2 min, considerably faster than ^{31}P MRS, breath-hold cine-MRI, and PET scans can practically be executed in people.

Moreover, the results of this study illustrate how hyperpolarized ^{13}C MRS/MRI could be useful to diagnose heart failure and to optimize its treatment.[25,30] We identified distinct profiles of substrate utilization based on markers acquired non-invasively with hyperpolarized ^{13}C MR (i.e. normal, reduced [^{13}C]glutamate production only, and both reduced [^{13}C]glutamate and [^{13}C]bicarbonate production). In future, other distinct profiles of ^{13}C-labelled tracer metabolism may emerge that correlate with cardiomyopathy stage and aetiology. The concept of metabolic stress testing, in which dobutamine stress is used to assess the heart's potential to increase carbohydrate oxidation at the level of the PDC to increase ATP production subsequently, could also play a role to identify stage-specific changes to metabolic flexibility. If this is the case, metabolic profiling with hyperpolarized ^{13}C MR may be useful for clinicians to select which patients could benefit from treatment with pharmacological agents that modulate metabolism, and, furthermore, may suggest which metabolic pathway may be the best to target[25,30,43] (i.e. trimetazidine[44] and carnitine palmitoyltransferase-1 inhibitors[39] to limit fatty acid oxidation, or glucagon-like peptide-1 agonists[10] to improve insulin sensitivity). Serial ^{13}C metabolic profiling may also be useful to monitor the efficacy of heart failure treatments, particularly metabolic modulators, but also including non-metabolic drugs and interventional therapies that improve cardiac efficiency.[5,6]

Conclusions

In summary, by applying hyperpolarized ^{13}C MRI and MRS to an experimental model of heart failure, we performed the first non-invasive measurements of cardiac pyruvate metabolism throughout disease pathogenesis, alongside measurement of myocardial energetics, structure, and function. At an early stage of disease, hyperpolarized ^{13}C MRS revealed an alteration to [^{13}C]glutamate production, concomitant with impaired cardiac function and energetics. Further, by using hyperpolarized ^{13}C MRI to measure [1-^{13}C]pyruvate oxidation by the PDC serially at frequent time points, we identified a temporal association between reduced pyruvate oxidation and the onset of overt heart failure. With the use of methods such as those presented here, it is possible that metabolic MR with hyperpolarized ^{13}C-labelled tracers will form an important part of both basic cardiovascular research and routine clinical diagnosis and treatment monitoring in cardiology.

Supplementary material

Supplementary material is available at *European Journal of Heart Failure* online.

Acknowledgements

The authors would like to thank Professor Sir George Radda, Professor E. Douglas Lewandowski, Professor Peter P. Liu, and Dr Nilesh Ghugre for engaging in many helpful discussions.

Funding

A Sir Henry Wellcome Post-doctoral Research Fellowship (to M.A.S.), the Heart and Stroke Foundation of Canada Canada Clinician scientist program phase 1 (grant to K.A.C.). The Canadian Institutes for Health Research (grant no. CIHR MOP84503), the Heart and Stroke Foundation of Canada (HSF NA7074), the Natural Sciences and Engineering Research Council of Canada (NSERC PGS-D).

Conflict of interest: A.P.C. is an employee of GE Healthcare. This work received research support from Medtronic and GE Healthcare. G.A.W. holds stock in GE Healthcare, the principal commercial developers of hyperpolarized ^{13}C techology, and is currently conducting research sponsored by this company. He has also received a speaker's honorarium from GE Healthcare within the past 12 months. C.H.C. receives research support from GE Healthcare who own many patents on DNP technology. D.J.T. has previously received equipment support from GE Healthcare and Oxford instruments. All other authors have no conflicts to decalre.

References

1. Neubauer S. The failing heart—an engine out of fuel. *N Engl J Med* 2007;**356**:1140–1151.
2. Stanley WC, Recchia FA, Lopaschuk GD. Myocardial substrate metabolism in the normal and failing heart. *Physiol Rev* 2005;**85**:1093–1129.
3. Neubauer S, Krahe T, Schindler R, Horn M, Hillenbrand H, Entzeroth C, Mader H, Kromer EP, Riegger GA, Lackner K, Ertl G. 31P magnetic resonance spectroscopy in dilated cardiomyopathy and coronary artery disease. Altered cardiac high-energy phosphate metabolism in heart failure. *Circulation* 1992;**86**:1810–1818.
4. Shen WQ, Asai K, Uechi M, Mathier MA, Shannon RP, Vatner SF, Ingwall JS. Progressive loss of myocardial ATP due to a loss of total purines during the development of heart failure in dogs—a compensatory role for the parallel loss of creatine. *Circulation* 1999;**100**:2113–2118.
5. Beanlands RS, Nahmias C, Gordon E, Coates G, deKemp R, Firnau G, Fallen E. The effects of beta(1)-blockade on oxidative metabolism and the metabolic cost of ventricular work in patients with left ventricular dysfunction: a double-blind, placebo-controlled, positron-emission tomography study. *Circulation* 2000;**102**:2070–2075.
6. Ukkonen H, Beanlands RS, Burwash IG, de Kemp RA, Nahmias C, Fallen E, Hill MR, Tang AS. Effect of cardiac resynchronization on myocardial efficiency and regional oxidative metabolism. *Circulation* 2003;**107**:28–31.
7. Sack MN, Rader TA, Park S, Bastin J, McCune SA, Kelly DP. Fatty acid oxidation enzyme gene expression is downregulated in the failing heart. *Circulation* 1996;**94**:2837–2842.

8. Razeghi P, Young ME, Alcorn JL, Moravec CS, Frazier OH, Taegtmeyer H. Metabolic gene expression in fetal and failing human heart. *Circulation* 2001;**104**: 2923–2931.
9. Lei B, Lionetti V, Young ME, Chandler MP, d'Agostino C, Kang E, Altarejos M, Matsuo K, Hintze TH, Stanley WC, Recchia FA. Paradoxical downregulation of the glucose oxidation pathway despite enhanced flux in severe heart failure. *J Mol Cell Cardiol* 2004;**36**:567–576.
10. Nikolaidis LA, Elahi D, Hentosz T, Doverspike A, Huerbin R, Zourelias L, Stolarski C, Shen YT, Shannon RP. Recombinant glucagon-like peptide-1 increases myocardial glucose uptake and improves left ventricular performance in conscious dogs with pacing-induced dilated cardiomyopathy. *Circulation* 2004;**110**: 955–961.
11. Opie LH, Knuuti J. The adrenergic-fatty acid load in heart failure. *J Am Coll Cardiol* 2009;**54**:1637–1646.
12. Osorio JC, Stanley WC, Linke A, Castellari M, Diep QN, Panchal AR, Hintze TH, Lopaschuk GD, Recchia FA. Impaired myocardial fatty acid oxidation and reduced protein expression of retinoid×receptor-alpha in pacing-induced heart failure. *Circulation* 2002;**106**:606–612.
13. Recchia FA, McConnell PI, Bernstein RD, Vogel TR, Xu X, Hintze TH. Reduced nitric oxide production and altered myocardial metabolism during the decompensation of pacing-induced heart failure in the conscious dog. *Circ Res* 1998;**83**: 969–979.
14. Taylor M, Wallhaus TR, Degrado TR, Russell DC, Stanko P, Nickles RJ, Stone CK. An evaluation of myocardial fatty acid and glucose uptake using PET with [18F]fluoro-6-thia-heptadecanoic acid and [18F]FDG in Patients with Congestive Heart Failure. *J Nucl Med* 2001;**42**:55–62.
15. Paolisso G, Gambardella A, Galzerano D, D'Amore A, Rubino P, Verza M, Teasuro P, Varricchio M, D'Onofrio F. Total-body and myocardial substrate oxidation in congestive heart failure. *Metabolism* 1994;**43**:174–179.
16. Nikolaidis LA, Sturzu A, Stolarski C, Elahi D, Shen YT, Shannon RP. The development of myocardial insulin resistance in conscious dogs with advanced dilated cardiomyopathy. *Cardiovasc Res* 2004;**61**:297–306.
17. Paternostro G, Camici PG, Lammerstma AA, Marinho N, Baliga RR, Kooner JS, Radda GK, Ferrannini E. Cardiac and skeletal muscle insulin resistance in patients with coronary heart disease. A study with positron emission tomography. *J Clin Invest* 1996;**98**:2094–2099.
18. Horowitz JD, Kennedy JA. Time to address the cardiac metabolic 'triple whammy' ischemic heart failure in diabetic patients. *J Am Coll Cardiol* 2006;**48**:2232–2234.
19. Budoff MJ, Gupta M. Radiation exposure from cardiac imaging procedures. *J Am Coll Cardiol* 2010;**56**:712–714.
20. Ingwall JS, Weiss RG. Is the failing heart energy starved? On using chemical energy to support cardiac function. *Circ Res* 2004;**95**:135–145.
21. Ardenkjaer-Larsen JH, Fridlund B, Gram A, Hansson G, Hansson L, Lerche MH, Servin R, Thaning M, Golman K. Increase in signal-to-noise ratio of >10,000 times in liquid-state NMR. *Proc Natl Acad Sci USA* 2003;**100**:10158–10163.
22. Golman K, Petersson JS, Magnusson P, Johansson E, Akeson P, Chai CM, Hansson G, Mansson S. Cardiac metabolism measured noninvasively by hyperpolarized 13C MRI. *Magn Reson Med* 2008;**59**:1005–1013.
23. Schroeder M, Cochlin L., Heather L., Clarke K., Radda G., Tyler D. *In vivo* assessment of pyruvate dehydrogenase flux in the heart using hyperpolarized carbon-13 magnetic resonance. *Proc Natl Acad Sci USA* 2008;**105**:12051–12056.
24. Merritt ME, Harrison C, Storey C, Jeffrey FM, Sherry AD, Malloy CR. Hyperpolarized 13C allows a direct measure of flux through a single enzyme-catalyzed step by NMR. *Proc Natl Acad Sci USA* 2007;**104**:19773–19777.
25. Schroeder MA, Clarke K, Neubauer S, Tyler DJ. Hyperpolarized magnetic resonance: a novel technique for the *in vivo* assessment of cardiovascular disease. *Circulation* 2011;**124**:1580–1594.
26. Schroeder MA, Atherton HJ, Ball DR, Cole MA, Heather LC, Griffin JL, Clarke K, Radda GK, Tyler DJ. Real-time assessment of Krebs cycle metabolism using hyperpolarized 13C magnetic resonance spectroscopy. *FASEB J* 2009;**23**: 2529–2538.
27. Lau AZ, Chen AP, Ghugre NR, Ramanan V, Lam WW, Connelly KA, Wright GA, Cunningham CH. Rapid multislice imaging of hyperpolarized 13C pyruvate and bicarbonate in the heart. *Magn Reson Med* 2010;**64**:1323–1331.
28. Golman K, in't Zandt R., Thaning M. Real-time metabolic imaging. *Proc Natl Acad Sci USA* 2006;**103**:11270–11275.
29. Lau A, Chen, Schroeder, Lam, Gu, Barry, Cunningham. Free-breathing cardiac and respiratory-gated imaging of hyperpolarized pyruvate and bicarbonate in the heart. *International Society of Magnetic Resonance in Medicine*. Montreal, Canada, 2011.
30. Malloy CR, Merritt ME, Sherry AD. Could 13C MRI assist clinical decision-making for patients with heart disease? *NMR Biomed* 2011;**24**:973–979.
31. Schroeder MA, Atherton HJ, Dodd MS, Lee P, Cochlin LE, Radda GK, Clarke K, Tyler DJ. The cycling of acetyl-coenzyme A through acetylcarnitine buffers cardiac substrate supply: a hyperpolarized 13C magnetic resonance study. *Circ Cardiovasc Imaging* 2012;**5**:201–209.
32. Atherton HJ, Schroeder MA, Dodd MS, Heather LC, Carter EE, Cochlin LE, Nagel S, Sibson NR, Radda GK, Clarke K, Tyler DJ. Validation of the *in vivo* assessment of pyruvate dehydrogenase activity using hyperpolarised (13) C MRS. *NMR Biomed* 2010;**24**:201–208.
33. Lau AZ, Chen AP, Cunningham CH. Integrated Bloch–Siegert B(1) mapping and multislice imaging of hyperpolarized (1) (3)C pyruvate and bicarbonate in the heart. *Magn Reson Med* 2012;**67**:62–71.
34. Di Lisa F, Fan CZ, Gambassi G, Hogue BA, Kudryashova I, Hansford RG. Altered pyruvate dehydrogenase control and mitochondrial free Ca2+ in hearts of cardiomyopathic hamsters. *Am J Physiol* 1993;**264**:H2188–H2197.
35. Atherton HJ, Dodd MS, Heather LC, Schroeder MA, Griffin JL, Radda GK, Clarke K, Tyler DJ. Role of pyruvate dehydrogenase inhibition in the development of hypertrophy in the hyperthyroid rat heart: a combined magnetic resonance imaging and hyperpolarized magnetic resonance spectroscopy study. *Circulation* 2011;**123**:2552–2561.
36. Pound KM, Sorokina N, Ballal K, Berkich DA, Fasano M, Lanoue KF, Taegtmeyer H, O'Donnell JM, Lewandowski ED. Substrate–enzyme competition attenuates upregulated anaplerotic flux through malic enzyme in hypertrophied rat heart and restores triacylglyceride content: attenuating upregulated anaplerosis in hypertrophy. *Circ Res* 2009;**104**:805–812.
37. Sorokina N, O'Donnell JM, McKinney RD, Pound KM, Woldegiorgis G, LaNoue KF, Ballal K, Taegtmeyer H, Buttrick PM, Lewandowski ED. Recruitment of compensatory pathways to sustain oxidative flux with reduced carnitine palmitoyltransferase I activity characterizes inefficiency in energy metabolism in hypertrophied hearts. *Circulation* 2007;**115**:2033–2041.
38. Caruso M, Maitan MA, Bifulco G, Miele C, Vigliotta G, Oriente F, Formisano P, Beguinot F. Activation and mitochondrial translocation of protein kinase Cdelta are necessary for insulin stimulation of pyruvate dehydrogenase complex activity in muscle and liver cells. *J Biol Chem* 2001;**276**:45088–45097.
39. Lee L, Campbell R, Scheuermann-Freestone M, Taylor R, Gunaruwan P, Williams L, Ashrafian H, Horowitz J, Fraser AG, Clarke K, Frenneaux M. Metabolic modulation with perhexiline in chronic heart failure: a randomized, controlled trial of short-term use of a novel treatment. *Circulation* 2005;**112**:3280–3288.
40. Halestrap AP, Price NT. The proton-linked monocarboxylate transporter (MCT) family: structure, function and regulation. *Biochem J* 1999;**343**:281–299.
41. Johannsson E, Lunde PK, Heddle C, Sjaastad I, Thomas MJ, Bergersen L, Halestrap AP, Blackstad TW, Ottersen OP, Sejersted OM. Upregulation of the cardiac monocarboxylate transporter MCT1 in a rat model of congestive heart failure. *Circulation* 2001;**104**:729–734.
42. Chen AP, Hurd RE, Schroeder MA, Lau AZ, Gu YP, Lam WW, Barry J, Tropp J, Cunningham CH. Simultaneous investigation of cardiac pyruvate dehydrogenase flux, Krebs cycle metabolism and pH, using hyperpolarized [1,2-(13)C2]pyruvate *in vivo*. *NMR Biomed* 2012;**25**:305–311.
43. Ardehali H, Sabbah HN, Burke MA, Sarma S, Liu PP, Cleland JG, Maggioni A, Fonarow GC, Abel ED, Campia U, Gheorghiade M. Targeting myocardial substrate metabolism in heart failure: potential for new therapies. *Eur J Heart Fail* 2012;**14**:120–129.
44. Kantor PF, Lucien A, Kozak R, Lopaschuk GD. The antianginal drug trimetazidine shifts cardiac energy metabolism from fatty acid oxidation to glucose oxidation by inhibiting mitochondrial long-chain 3-ketoacyl coenzyme A thiolase. *Circ Res* 2000; **86**:580–588.